Applied Catalysis B: Environmental 343 (2024) 123554

Contents lists available at ScienceDirect

Applied Catalysis B: Environmental

journal homepage: www.elsevier.com/locate/apcatb

# Synergetic multiple free radicals lower the organohalide conversion barrier and potentiate effective contaminant mineralization

Jun Zhang [a,b,*], Songying Qu [c,**]

[a] Institute of Environment and Ecology, Tsinghua Shenzhen International Graduate School, Tsinghua University, Shenzhen 518055, China
[b] Center for Water and Ecology, School of Environment, Tsinghua University, Beijing 100084, China
[c] School of Energy and Environment, City University of Hong Kong, 999077 Hong Kong, China

ARTICLE INFO

*Keywords:*
Multiple free radicals
Halogen organic pollutants
Photoelectrocatalytic platform
Conversion energy barrier
Intermediate accumulation

ABSTRACT

Here we investigated the synergetic multiple free radicals (atomic hydrogen (H*), superoxide anion ($\bullet O_2^-$), and hydroxyl radicals (•OH)) in enhancing removal efficiencies of the halogen organic pollutants, such as p-chlorophenol (4-CP). A $TiO_2$ photoanode and a palladium and carbon layer co-modified $Cu/Cu_2O/CuO$ ($Cu_xO$@C/Pd) photocathode were combined to construct a photoelectrocatalytic platform that enabled the synchronous production of multiple free radicals. It was found that the conversion and mineralization rates of 4-CP were up to ~0.044 $min^{-1}$ and ~71.3% respectively, representing an increase of ~4.3 times and ~2.1 times compared to conventional •OH mediated oxidation. Theoretical calculations and experiments indicated that the conversion barrier of 4-CP was significantly reduced through the redox synergies of H* and •OH and the simultaneous nucleophilic-electrophilic addition of $\bullet O_2^-$ effectively inhibited the accumulation of benzoquinone intermediates. This work is beneficial for the study and application of advanced oxidation processes mediated by multiple free radicals.

## 1. Introduction

Advanced oxidation processes (AOPs), with hydroxyl radicals (•OH) as the core, are state-of-the-art technologies for organic wastewater treatment [1–3]. The •OH boasts an exceptionally robust oxidizing capacity, facilitating the decomposition of organic pollutants into innocuous inorganic substances ($H_2O$, $CO_2$, and so on) through a series of chain oxidation reactions [4–6]. Over the past few decades, researchers have dedicated themselves to the construction of homogeneous and heterogeneous catalytic systems capable of efficient •OH generation [7–10]. A consensus has emerged from these studies that augmenting the concentration of •OH is the only effective strategy to enhance pollutant degradation efficiency, as environments rich in •OH are conducive to collisions between •OH and pollutants [11–13]. All the while, however, another critical issue has been overlooked, that is, the redox properties of pollutants continually shift throughout the degradation process, i.e., intermediates at various stages demonstrate differing Lewis acid-base properties. Thus, a system reliant on one-component •OH, possessing only oxidizing property, falls short of fully addressing the entire catalytic reaction process.

Utilizing the degradation of halogen organic pollutants (HOPs) as a prototype, •OH mediated oxidation struggles to effectively remove HOPs from water, characterized by slow conversion and low mineralization rates (Scheme 1A) [14–19]. The likely explanation is that the carbon atoms in HOPs exhibit weak electron donating abilities due to the strong electronegativity of halogen substituent groups. This results in a high conversion barrier in the process of electrophilic addition of HOPs by •OH, consequently leading to a low conversion rate. Moreover, HOPs, primarily halogenated aromatic hydrocarbons, are readily converted to benzoquinone (BQ) intermediates [10,14]. This formed BQ is challenging to further oxidize by •OH due to the high reaction barrier, attributed to the strong polarity of carbonyl groups (C═O) causing an uneven electron cloud distribution in BQ. This results in two adjacent carbon atoms having completely opposing abilities to gain or lose electrons. The accumulation of BQ directly leads to a low mineralization rate. However, our latest works have tentatively demonstrated that the synergy of multiple free radicals holds promise for effectively removing HOPs (Scheme 1B) [20,21]. The conversion barriers of HOPs can be

* Corresponding author at: Institute of Environment and Ecology, Tsinghua Shenzhen International Graduate School, Tsinghua University, Shenzhen 518055, China.
** Corresponding author.
*E-mail addresses:* zhangboyu2016@sz.tsinghua.edu.cn (J. Zhang), qusongying163@163.com (S. Qu).

https://doi.org/10.1016/j.apcatb.2023.123554
Received 4 August 2023; Received in revised form 21 November 2023; Accepted 22 November 2023
Available online 25 November 2023

significantly reduced through a redox synergistic process of atomic hydrogen (H*)-initiating nucleophilic hydrodehalogenation, followed by •OH electrophilic oxidation of critical intermediates. Additionally, the introduction of the superoxide anion ($•O_2^-$) will effectively inhibit BQ accumulation. This effect can be attributed to the simultaneous roles of $•O_2^-$ as both an electron donor and acceptor, and its ability to electrophilically and nucleophilically add to BQ synchronously and degrade it. The breakdown products can be further oxidized by •OH until they are completely mineralized. Therefore, for efficient HOPs removal, it is essential that H* , $•O_2^-$, and •OH are simultaneously generated and coexist within the reaction system.

Based on the analyses presented, we systematically demonstrated for the first time the feasibility and underlying mechanism of applying such advanced oxidation platform mediated by multiple free radicals (H*, $•O_2^-$, and •OH) for the effective conversion and mineralization of HOPs by theoretical calculation (Scheme 1C). We delved into potential reaction paths, variations in free energy, electron density distribution, and charge transfers associated with HOPs, BQ, and other critical intermediates. Subsequently, we purposefully designed and constructed an innovative photoelectrocatalytic (PEC) system, consisting of a $TiO_2$ photoanode and palladium and carbon layer co-modified $Cu/Cu_2O/CuO$ ($Cu_xO$@C/Pd) photocathode. The •OH generated on the $TiO_2$ surface via one-electron water oxidation reaction (WOR) (Eq. 1), while the $Cu_xO$@C/Pd simultaneously produced H* and $•O_2^-$ via hydrogen fixation (Volmer) (Eq. 2) and molecular oxygen activation (MOA) (Eq. 3) processes, respectively (Scheme 1D) [22–26]. Controlled experiments focusing primarily on degradation kinetics and pathways in systems mediated by different free radicals were conducted to further corroborate the theoretical calculation results. In parallel, a continuous-flow PEC reactor, featuring the synergy of multiple free radicals, was developed to broaden its practical application. This included a detailed investigation of effluent safety, operational stability, and nonspecific substrate feasibility etc. Finally, we systematically evaluated the advantages of such a highly efficient electrochemical water purification system mediated by multiple free radicals in terms of reducing energy consumption, greenhouse gas emissions, and impacts on resources, ecosystems, and human health, as outlined in a comprehensive life cycle assessment (LCA) (Scheme 1E). Overall, our findings underscore the significance of regulating free radical types in AOPs.

$$H_2O + h^+/TiO_2 \rightarrow •OH + H^+ + e^- \quad (1)$$

$$H_2O + e^-/Cu_xO@C/Pd \rightarrow H^*/Cu_xO@C/Pd + OH^- \quad (2)$$

$$O_2 + e^-/Cu_xO@C/Pd \rightarrow •O_2^- \quad (3)$$

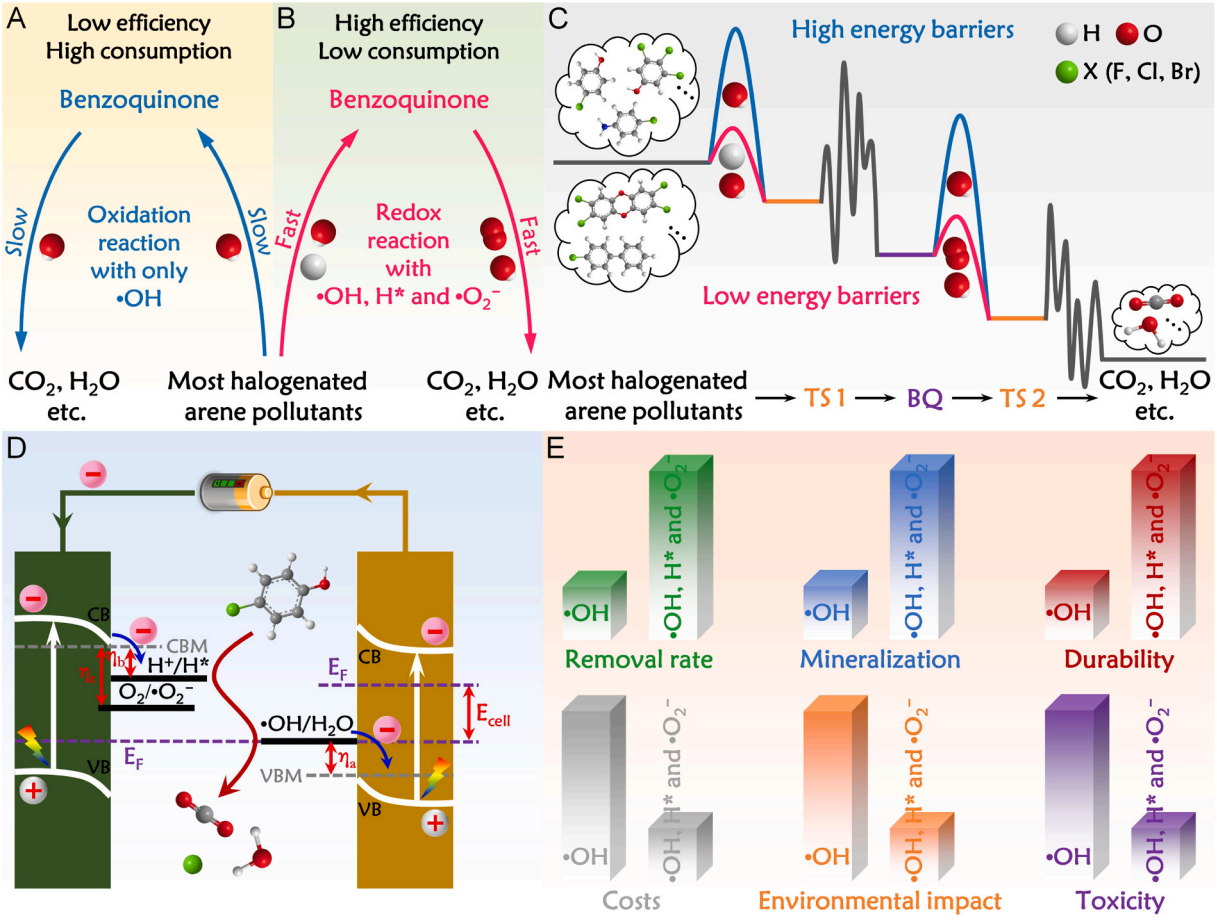


**Scheme S1. .** Design considerations. Comparison of the HOPs degradation efficiency in systems mediated by (a) one-component •OH and (b) innovative multiple free radicals, respectively, illustrating that (c) the synergy of multiple free radicals dramatically lowered conversion barriers of HOPs and BQ intermediate and thus potentiated effective HOPs conversion and mineralization; (d) Working principle (reaction mechanism) of PEC system with dual-photoelectrodes for synchronously producing multiple free radicals and efficiently decomposing HOPs; $\eta_a$ denoted the anodic overpotential for $•OH/H_2O$; $\eta_b$ denoted the cathodic overpotential for $H^+/H_2$; $\eta_c$ denoted the cathodic overpotential for $O_2/•O_2^-$; $E_F$ denoted the Fermi level; $E_{cell}$ denoted the bias voltage needed to operate the overall cell; VB denoted the valence band; CB denoted the conduction band; VBM denoted the valence band maximum; CBM denoted the valence band minimum; (e) A lot of advantages of the system mediated by multiple free radicals compared to one-component •OH mediated system for water purification.

## 2. Materials and methods

### 2.1. Photoelectrodes synthesis

All reagents were purchased from Aladdin reagent Co., LTD (Shanghai, China) and used directly without further treatment. The $TiO_2$ photoanode was prepared by a hydrothermal etching coupled calcination process. A piece of titanium foam (length × width × height = 2 × 2 × 0.1 cm) was immersed in 30 mL 4 M sodium hydroxide (NaOH) solution and then hydrothermal-treated at 180° for 6 h. After that, the electrode was repeatedly rinsed with ultrapure water and immersed in 50 mL 1 M nitric acid ($HNO_3$) solution for 24 h. Finally, the electrode was put into the Muffle furnace and calcined at 450° for 2 h, and then the $TiO_2$ photoanode has been successfully synthesized. The preparation process of palladium-carbon co-modified Cu/$Cu_2O$/CuO ($Cu_xO$@C/Pd) photocathode has been described in detail in our previous studies. A piece of copper foam (length × width × height = 2 × 2 × 0.1 cm) was put into the Muffle furnace and calcined at 500° for 2 h to obtain $Cu_xO$ electrode. Then the $Cu_xO$ was used as work electrode, and a Pt foil and an Ag/AgCl acted as counter and reference electrodes, respectively. An aqueous solution composed of 0.1 g $L^{-1}$ carbon quantum dots (CQDs) and 5 mM sodium sulfate ($Na_2SO_4$) was used as the deposition electrolyte. All electrodes were placed in a single chamber electrochemical cell fitted with 100 mL pre-made electrolyte, and a 0.6 V (vs. Ag/AgCl) bias potential was applied and ran continuously for 60 min to synthesize $Cu_xO$@C. The $Cu_xO$@C was further used as work electrode to electrodeposit palladium (Pd) nanoparticles to prepare $Cu_xO$@C/Pd, in which the electrolyte was replaced with 0.1 M palladium chloride ($PdCl_2$) aqueous solution, and the bias potential was set to − 0.4 V (vs. Ag/AgCl).

### 2.2. Characterization

The morphology and phase structure of as-prepared electrodes were investigated by scanning electron microscopy (SEM) (GeminiSEM 500), X-ray diffractometer (XRD) (Bruker D8 Discover), and Raman spectrograph (LabRAM HR Evolution). X-ray photoelectron spectroscopy (XPS) (ESCALAB 250Xi) was used to analyze the surface chemical states and elements of electrodes. UV—Vis diffuse reflectance spectrum (DRS) (Hitachi U-3900) and incident photon-to-electron conversion efficiency (IPCE) were performed to assess the photoelectric conversion characteristic of electrodes. Electron spin resonance (ESR) spectra of free radicals were recorded on a JEOL FA-200 spectrometer using the spin-trap reagent DMPO (5,5-dimethyl-1-pyrroline N-oxide, Sigma).

### 2.3. Experimental setup

All electrochemical experiments were conducted using a standard three-electrode or two-electrode system on the electrochemical workstation (AUTOLAB PGSTAT302N, METROHM, Switzerland). A 300 W xenon lamp (CEL-HXF300-T3, China Education Au-light, China) was used as the light source and its emission spectrum was shown in Fig. S1. The used work electrodes included $TiO_2$, $Cu_xO$@C/Pd, and Pt foil. The Ag/AgCl was acted as the reference electrode. The p-chlorophenol (4-CP) was selected as the target pollutant and its initial concentration was set to 10 mg $L^{-1}$. Meanwhile, the solution contained 0.1 M $Na_2SO_4$ to ensure good electrical conductivity. The photoelectrocatalytic (PEC) water purification device was constructed by integrating the $TiO_2$ photoanode and $Cu_xO$@C/Pd photocathode (Fig. S2). In the experiment, a certain volume of reaction solution was sampled regularly and filtered through a 0.45 μm membrane before detection. A continuous-flow column PEC reactor was constructed successfully. Such a complete set of equipment included influent/effluent tanks, pump, light source, direct-current (DC) power supply, and most importantly, column PEC reactor (Fig. S3). The light source was a single-head light-emitting diode (LED) ultraviolet tube (ZW14D15W-Z287, PHILP, Netherlands) and its output power and maximum emission wavelength was 14 W and 275–320 nm, respectively. The $TiO_2$‖$Cu_xO$@C/Pd module acted as the core component and was mounted in a column PEC unit, in which the semicircular tubular $TiO_2$ photoanode and the semicircular tubular $Cu_xO$@C/Pd photocathode were wrapped symmetrically on both sides of the central ultraviolet tube.

### 2.4. Analytical methods

A high-performance liquid chromatography (HPLC) (Alliance e2695) equipped with a 4.6 × 250 mm, 5 μm Venusil HILIC column was operated to detect the concentration of model organic pollutants. The produced intermediates of halogen organic pollutants (HOPs) degradation were identified by a quadrupole time-of-flight liquid chromatography-mass spectrometry (Waters Xevo G2 QTof LC-MS). A TOC-L analyzer was used to measure the mineralization degree of emerging pollutants. The released Pd, Cu, and Ti contents were determined via an inductively coupled plasma mass spectrometry (ICP-MS) (Agilent 7800). In the quenching experiments of reactive species, the 2,2,6,6-tetramethyl-1-piperidinyloxy (TEMPOL), tertiary butanol (TBA), Fe(II)-EDTA, sodium oxalate, Ar, and methanol (MeOH) were used as trapping agent for superoxide anion ($\bullet O_2^-$), atomic hydrogen (H*) and •OH, hydrogen peroxide ($H_2O_2$), hole ($h^+$), $O_2$, and •OH and sulfate radical ($SO_4\bullet^-$) respectively.

To investigate the 4-CP degradation efficiency and unveiling synergistic redox mechanism in •OH, H* and $\bullet O_2^-$ co-mediated PEC systems, the concentration level of •OH was regulated precisely by adding different quantities of quench agent (sodium oxalate) into $TiO_2$‖$Cu_xO$@C/Pd PEC system to ensure the same steady-state concentration of •OH in •OH mediated, •OH and H* co-mediated, •OH and $\bullet O_2^-$ co-mediated, and •OH, H* and $\bullet O_2^-$ co-mediated PEC systems. The concentration level of $\bullet O_2^-$ by adding different quantities of quench agent (TEMPOL) into $TiO_2$‖$Cu_xO$@C/Pd PEC system to ensure the same steady-state concentration of $\bullet O_2^-$ in $\bullet O_2^-$ mediated, $\bullet O_2^-$ and H* co-mediated, •OH and $\bullet O_2^-$ co-mediated, and •OH, H* and $\bullet O_2^-$ co-mediated PEC systems. Similarly, the Ar was used as the quench agent to precisely regulate the concentration level of H* in $TiO_2$‖$Cu_xO$@C/Pd PEC system.

DMPO was applied as the trapping agent and could react with $\bullet O_2^-$, •OH, and H* to form the DMPO-$O_2$, DMPO-OH, and DMPO-H paramagnetic adducts, respectively. The contents of produced $H_2O_2$ were detected via the iodometric method. The relative amount of H* was analyzed by cyclic voltammetry (CV) method. The •OH were quantitatively analyzed through fluorescence (FS) using benzoic acid (BA) as a probe. The $\bullet O_2^-$ concentrations were detected with 2,3-Bis-(2-methoxy-4-nitro-5-sulfophenyl)− 2 H-tetrazolium-5-carboxanilide (XTT) as probe on UV—Vis and simultaneously reexamined via FS using MCLA (2-methyl-6-(4-methoxyphenyl)− 3, 7-dihydroimidazo [1, 2-a] pyrazin-3(7 H)-one) as a probe.

The Toxicity Estimation Software Tool (T.E.S.T.) was conducted to evaluate the acute toxicity and mutagenicity of HOPs and its degradation intermediates by quantitative structure activity relationship (QSAR) predication. The acute toxicities were evaluated by the LC50 of fathead minnow (the concentration of a chemical that causes 50% fathead minnow to die after 96 h). In addition, the cytotoxicity assay further performed via investigate the growth inhibition assays using luminescent bacteria as model, in-vitro antibacterial assays using Escherichia coli (*E. coli*, gram-negative) and Staphylococcus aureus (*S. aureus*, gram-positive) as models, and teratogenicity analyses using zebrafish embryo as model after adding HOPs and its degradation intermediates.

Electric energy consumptions (KWh $g^{-1}$) for HOPs removal were calculated via the equation as follows: EC = UIt/W, where U denotes applied potential (V vs. RHE), I denotes measured current (A), t denotes reaction time (h), and W denotes weight (of HOPs and DOC, respectively). The life cycle assessment was performed according to the ISO

14040 and ISO 14044 standards by IKE Environmental Technology Co. Ltd., and the background data came from the Chinese Life Cycle Database (CLCD). The CLCD included more than 600 life cycle inventory datasets for raw materials, chemicals, energy, transportation, and waste treatment. Here, the electric energy consumption was correspondingly converted to primary energy demand (PED, standard coal eq./kg), global warming potential (GWP, $CO_2$ eq./kg), and US environmental prices (US$).

## 3. Results and discussion

### 3.1. Theoretical calculation

Theoretical calculations were conducted to predict the feasibility of using a multiple free radicals mediated system for highly efficient HOPs removal (Fig. 1 and Fig. S4). Theoretical conversion pathways of HOPs (using p-chlorophenol (4-CP) as an example) and corresponding Gibbs free energy changes ($\Delta G$) in •OH mediated and H* , •OH co-mediated systems were calculated and compared (Fig. 1A—B). There was a high reaction energy barrier (~2.51 eV) in the process of 4-CP conversion mediated by •OH, which was the immediate cause of the inefficiency in 4-CP conversion. In contrast, the synergistic action of H* and •OH resulted in efficient 4-CP conversion because of the steadier $\Delta G$. The H* initiated nucleophilic hydrodechlorination followed by •OH electrophilic oxidization of the critical dechlorination intermediate, in which the reaction energy barrier was as low as ~0.91 eV. Theoretical conversion pathways of the BQ intermediate and corresponding $\Delta G$ in •OH mediated and $\bullet O_2^-$ mediated systems were calculated and compared (Fig. 1**C**—**D**). There was a high reaction energy barrier (~2.12 eV) in the process of BQ conversion mediated by •OH, which was the immediate cause of BQ accumulation. In contrast, the reaction energy barrier hugely reduced to ~1.42 eV when using $\bullet O_2^-$ to attack and convert the BQ. The $\bullet O_2^-$ acted as an electron donor and acceptor simultaneously, and electrophilic and nucleophilic addition to BQ occurred synchronously, with the whole path showing gentle energy changes. The ball-and-stick model, electron density, difference charge density, lowest unoccupied molecular orbital (LUMO), and highest occupied molecular orbital (HOMO) of 4-CP, BQ, and critical intermediates were all displayed in Fig. 1E. The electrons were concentrated in the chlorine and hydroxyl groups in 4-CP, resulting in carbon atoms that were extremely electron-deficient, further evidenced by the LUMO and HOMO analyses. This made it difficult for the carbon atoms in 4-CP to provide electrons for •OH, resulting in weak electron transfer from 4-CP to •OH. By contrast, the electron-rich H* was easier to bond to the chlorine group (Cl—H), resulting in a strong electron transfer from H* to 4-CP and significantly stretching the C—Cl bond length. The critical dechlorination intermediate ($C_6H_5O$) tended to accept a •OH instead of H* because the carbon atoms lacking chlorine group showed a strong electronic donation ability, evidenced by the electron density distribution, LUMO, and HOMO analyses. The electron density distribution in BQ was extremely uneven due to the existence of the C═O bond, resulting in carbon atoms in C═O being extremely electron-deficient compared to the adjacent carbon atoms, and thus these two adjacent carbon atoms showed completely opposite redox properties.

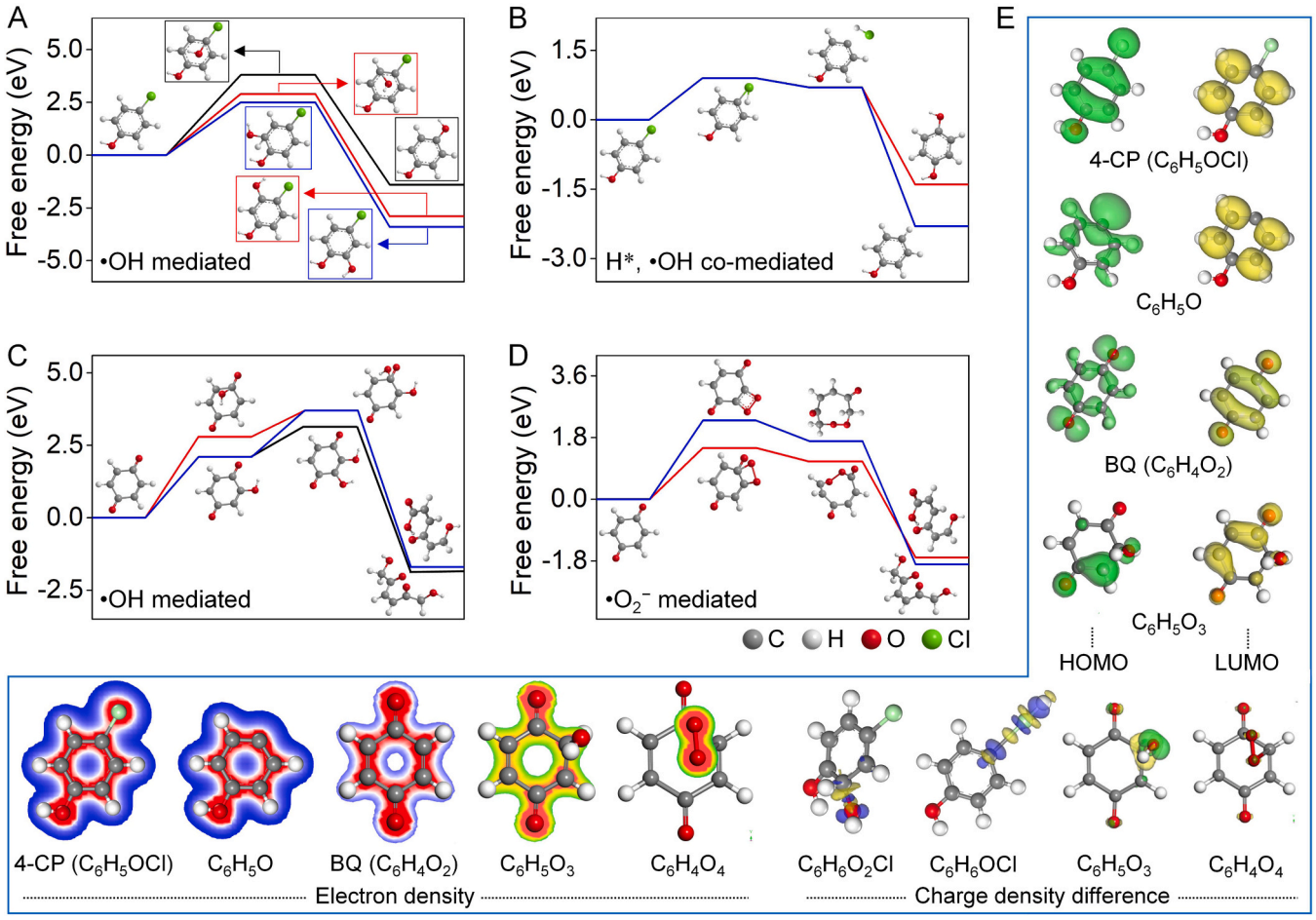


**Fig. 1.** Theoretical calculation. The conversion pathways of 4-CP and corresponding Gibbs free energy changes ($\Delta G$) in the (A) •OH mediated and (B) H* , •OH co-mediated systems, respectively; The conversion pathways of BQ and corresponding $\Delta G$ in the (C) •OH mediated and (D) $\bullet O_2^-$ mediated systems, respectively; (E) Ball-and-stick model, electron density, difference charge density, LUMO, and HOMO of 4-CP, critical intermediates, BQ, •OH additive BQ, and $\bullet O_2^-$ additive BQ.

The carbon atoms capable of electron donation were closely connected to the carbon atoms capable of electron acceptance, as evidenced by the LUMO and HOMO positions. When the •OH was added to the carbon atoms adjacent to the C═O bond in BQ, the electron density of the carbon atoms in the C═O bond was further reduced, and the LUMO and HOMO positions changed significantly, which was not conducive to subsequent electrophilic addition and ring opening. In contrast, the addition of $•O_2^-$ equalized the electron distribution and significantly stretched the C—C bond length, facilitating subsequent ring opening. From a thermodynamic perspective, the synergistic process based on multiple free radicals (H*, $•O_2^-$, and •OH) could more effectively convert and mineralize 4-CP compared to oxidative degradation by one-component •OH. This synergistic process was proved to be more sustainable and economically viable for the treatment of wastewater containing HOPs.

### 3.2. Construction and characterization of multiple free radicals production platform

According to our previous researches, the combination of a $TiO_2$ photoanode and $Cu_xO$@C/Pd photocathode to construct a $TiO_2$‖$Cu_xO$@C/Pd PEC platform theoretically enables the synchronous production of multiple free radicals in-situ, consisting of H* , $•O_2^-$, and •OH (Fig. 2A) [21,27]. Specifically, the photoelectrodes were photo-excited to generate electron-hole pairs, which were spatially separated by an external circuit under low potential (Fig. S5). Subsequently, the remaining holes in $TiO_2$ oxidized $OH^-$ to •OH, while the electrons gathered in $Cu_xO$@C/Pd reduced $H^+$ and $O_2$ to H* and $•O_2^-$, respectively. Based on this analysis, we separately fabricated the $TiO_2$ photoanode and $Cu_xO$@C/Pd photocathode and characterized their morphology, phase structure, and surface chemical state in detail using scanning electron microscopy (SEM) (Fig. 2B), X-ray diffraction (XRD), Raman spectroscopy, and X-ray photoelectron spectroscopy (XPS) etc. (Figs. S6–S9). The corresponding analyses and discussion can be found in the Supporting Information. Furthermore, the as-prepared $TiO_2$ and $Cu_xO$@C/Pd showed excellent photoelectric conversion performances, as evidenced by the diffuse reflection spectra (DRS) (Fig. 2C), incident photo-to-current conversion efficiency (IPCE), and transient linear sweep voltammetry (LSV) photocurrent tests (Fig. 2D). The band gap of $TiO_2$ was ~3.10, implying that the light with wavelengths less than 400 nm could effectively excite $TiO_2$ to generate •OH. The modification of carbon layer and Pd effectively enhanced the light absorption of $Cu_xO$ in the wavelength range less than the absorption edge, which was beneficial to produce more photoelectrons for free radicals' generation. Notably, the onset potential for the occurrence of $TiO_2$ photocurrent was significantly lower than that of $Cu_xO$@C/Pd. This indicates that the $TiO_2$ is ideally suited to pair with $Cu_xO$@C/Pd for constructing a dual-photoelectrode PEC platform, delivering high operational efficiency under low bias potential (Fig. S10) [28–30]. Consequently, the $TiO_2$‖$Cu_xO$@C/Pd PEC system exhibited a larger photocurrent density (~2.0 mA $cm^{-2}$) and a smaller electrochemical impedance than any individual half-reaction (Fig. S11). Electron spin resonance (ESR) revealed that the abundant available electrons and holes in $TiO_2$‖$Cu_xO$@C/Pd triggered the formation of numerous H* , $•O_2^-$, and •OH through mixed reaction processes, even under ambient conditions (Fig. 2E). The typical nine-line ESR signal of the DMPO-H* adduct and

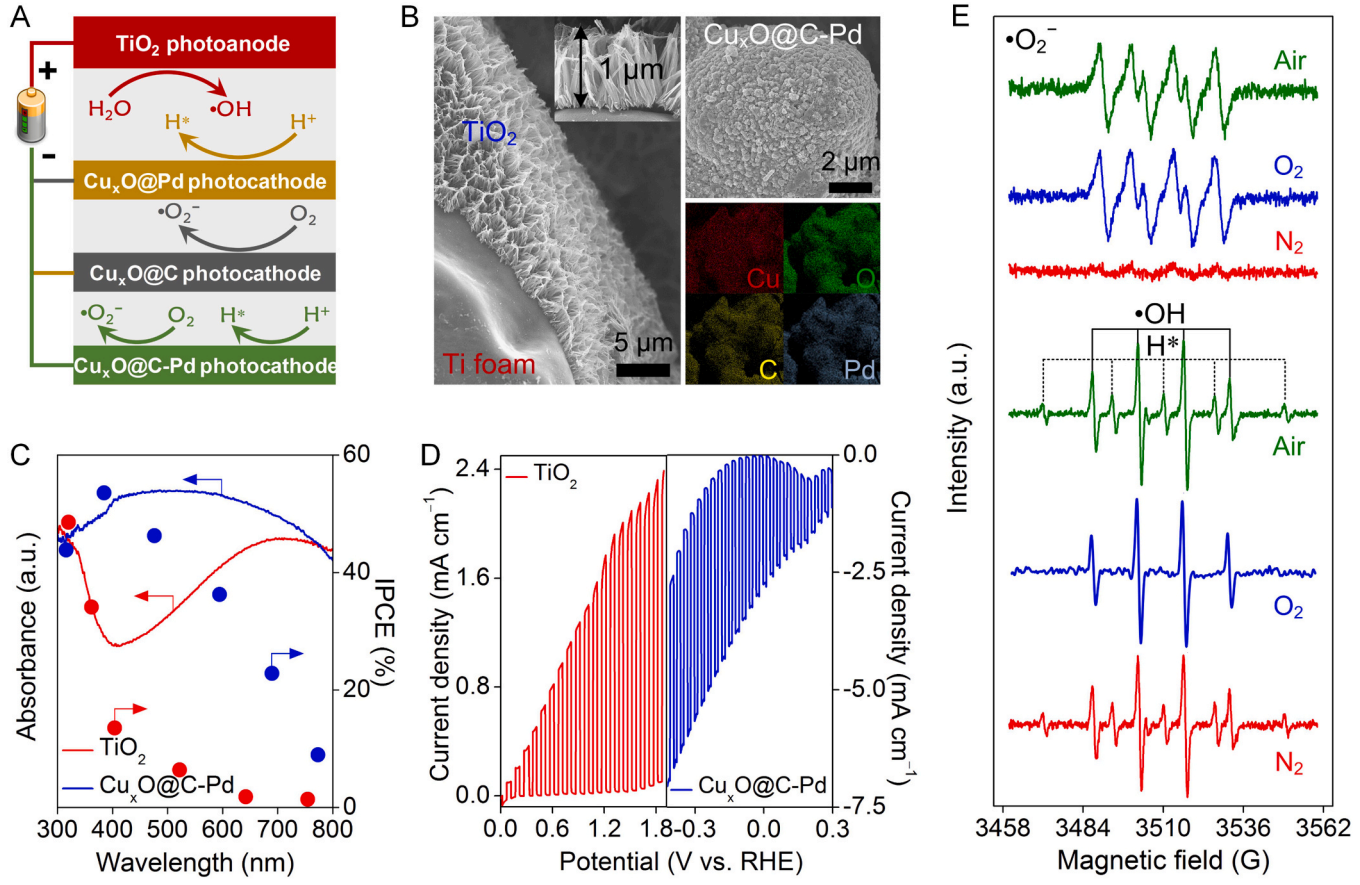


**Fig. 2.** Construction and characterization of $TiO_2$‖$Cu_xO$@C/Pd PEC platform. (A) Schematic diagram of $TiO_2$‖$Cu_xO$@C/Pd PEC system for synchronously generating H* , $•O_2^-$, and •OH; (B) SEM and EDX-mapping images of $TiO_2$ and $Cu_xO$@C/Pd; (C) UV—Vis DRS and IPCE tests of $TiO_2$ and $Cu_xO$@C/Pd; (D) Time-resolved LSV curves of $TiO_2$ and $Cu_xO$@C/Pd; (E) ESR spectra of H* , $•O_2^-$, and •OH recorded on $TiO_2$‖$Cu_xO$@C/Pd platform under $N_2$/$O_2$/air-saturated conditions. Experimental conditions: applied voltage (1.2 V), electrolyte (0.1 M $Na_2SO_4$), temperature (25 °C), light irradiation.

four-line ESR signal of the DMPO-•OH adduct were distinctly observed, although some overlap occurred, and the six-line ESR signal of the DMPO-•$O_2^-$ adduct was simultaneously captured [31–33]. It was worth mentioning that there was no characteristic peak of DMPO-$SO_4$•$^-$ adduct, indicating the nonexistence of sulfate radical ($SO_4$•$^-$) in current system. Meanwhile, the specific concentrations of H* , •$O_2^-$, and •OH were determined by fluorescence/high performance liquid chromatography analyses (Fig. S12).

### 3.3. Performance, pathway, and mechanism of HOPs removal in system mediated by multiple free radicals

Upon successfully constructing the $TiO_2$||$Cu_xO$@C/Pd PEC platform, capable of generating multiple free radicals (H*, •$O_2^-$, and •OH) synchronously in-situ, we proceeded to investigate the vital significance of this synergistic action of multiple free radicals on the rapid and comprehensive removal of HOPs. We initially aimed to experimentally confirm the beneficial effects of this synergy on the degradation of 4-CP [21,34]. It was clear that a change in 4-CP concentration from 0 to 100 mg $L^{-1}$ caused the signal intensities of •OH, H* , and •$O_2^-$ to gradually diminish in the system mediated by multiple free radicals, with attenuation rates significantly more rapid than those observed in the systems mediated by one/two-component free radicals (Fig. 3A—C). These results suggested that efficient 4-CP removal could only be achieved through the synergistic process of multiple free radicals. Subsequently, we quantitatively revealed the internal relationship between 4-CP removal and the concentration of multiple free radicals. As shown in Fig. S13, any increase in the concentration of one type of free radical, whether •OH (from 0.0 to 2.1 mM), H* (from 0.0 to 1.0 relative intensity), or •$O_2^-$ (from 0.0 to 2.1 mM), could significantly enhance the rate of 4-CP conversion, but not linearly. Meanwhile, the combinations of H* and •$O_2^-$ or •OH and •$O_2^-$ only slightly improved the 4-CP conversion rate and did not alter the nonlinear relationship. In contrast, the combination of •OH and H* straightened the growth curve. This implied that the synergy of •OH and H* not only significantly improved the 4-CP conversion rate, but also enabled a linear growth of the reaction rate with increasing the concentrations of •OH and H* . These results conclusively proved that •OH and H* were essential for rapid 4-CP conversion, but •$O_2^-$ was dispensable during the initial 4-CP conversion. Furthermore, increasing the concentration of one-component •OH could somewhat enhance the mineralization efficiency, but the effect was not significant (Fig. S14). While increasing the concentrations of one-component H* or •$O_2^-$ had barely any effect on improving mineralization efficiency. Also, the combinations of H* and •OH or H* and •$O_2^-$ only slightly improved mineralization efficiency, without causing a fundamental change. However, combining •$O_2^-$ and •OH together could remarkably enhance mineralization efficiency, which demonstrated a linear growth with the increase of •$O_2^-$ and •OH concentrations. These results confirmed that •OH and •$O_2^-$ were essential for effective 4-CP mineralization, while H* was powerless in this process. In addition, we have investigated and confirmed that there was no $SO_4$•$^-$ involved in the reaction process (Fig. S15).

As expected, the experimental results demonstrated that the synergy of multiple free radicals not only possessed a rapid 4-CP conversion rate ($k_{obs}$ = ~0.044 $min^{-1}$), but also displayed a notably high mineralization efficiency (DOC removal, ~71.3%) at the same time. This performance

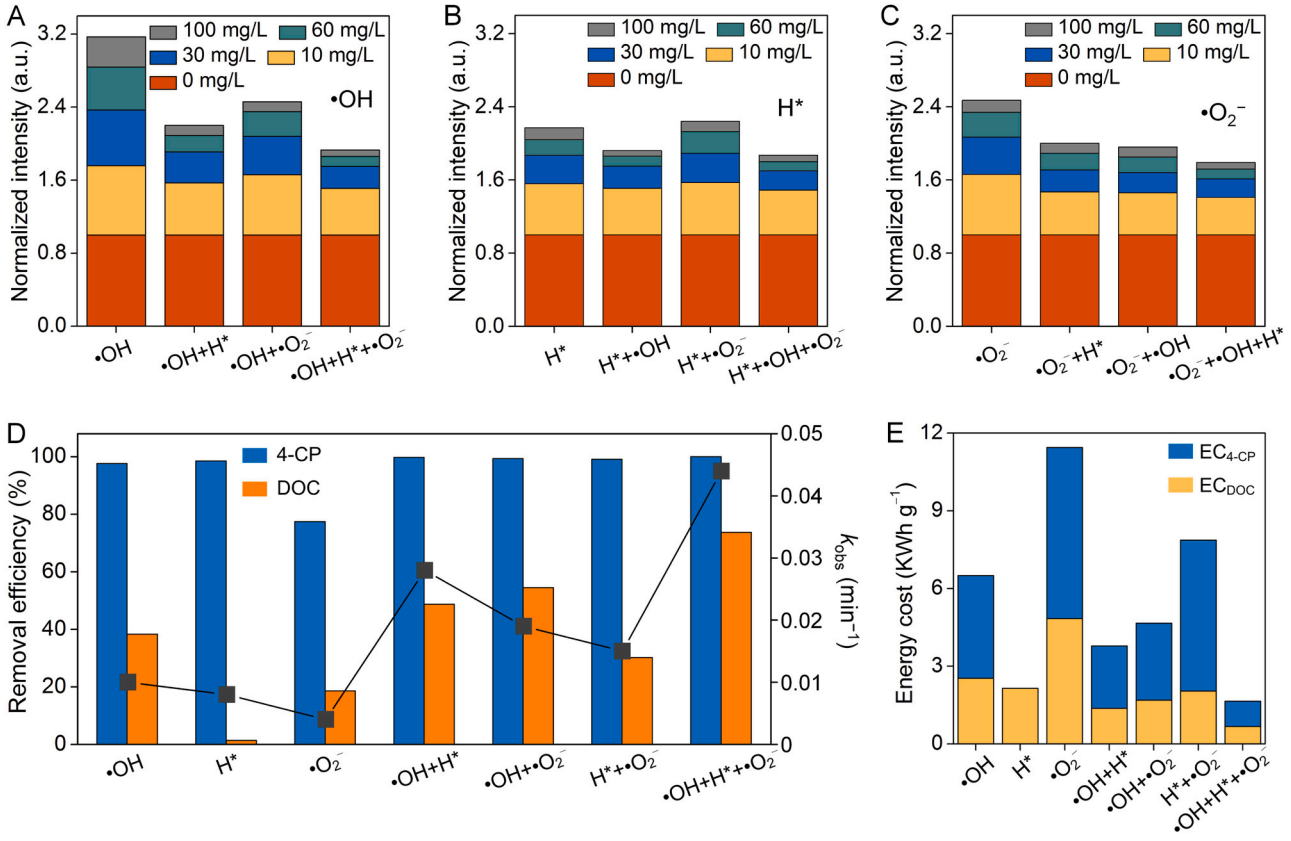


**Fig. 3.** Performance of 4-CP removal in $TiO_2$||$Cu_xO$@C/Pd PEC system. (A—C) Quantitative analyses of the synergy of multiple free radicals for 4-CP removal; Changes in the normalized ESR signal intensities of •OH, H* , and •$O_2^-$ in H* -mediated, •OH-mediated, •$O_2^-$-mediated, •OH and H* co-mediated, •$O_2^-$ and H* co-mediated, •OH and •$O_2^-$ co-mediated, and •OH, H* , and •$O_2^-$ co-mediated systems, respectively, with the 4-CP concentration increasing from 0 to 100 mg $L^{-1}$; (D) Conversion rate and mineralization efficiency of 4-CP in different systems; (E) Electric energy consumption of conversion and mineralization of 4-CP in different systems. All results were taken from the average of triplicate experiments. Experimental conditions: applied voltage (1.2 V), electrolyte (0.1 M $Na_2SO_4$), 4-$CP_0$ (10 mg $L^{-1}$), air condition, temperature (25 °C), light irradiation.

was far superior to other systems mediated by one/two-component free radicals (Fig. 3**D**). Consequently, the system mediated by multiple free radicals required significantly less electric energy for 4-CP conversion and mineralization compared to other systems mediated by one/two-component free radicals (Fig. 3**E**). In addition to these advantages, another critical aspect was that the system mediated by multiple free radicals could effectively inhibit the formation of electrode fouling. It is well known that organic pollutants in the bulk solution, including residual HOPs and accumulated intermediates, easily adhere strongly to the electrode, forming high-resistance polymers that obstruct the reactive sites on the electrode surface, resulting in electrode deactivation [10,35]. Tmiely elimination of these polymers to refresh the electrode surface or even inhibit their formation is critical to avoid electrode poisoning and ensure the normal operation of the system. It was gratifying to find that the system mediated by multiple free radicals in this work showed excellent electrode anti-fouling performance. As depicted in Fig. S16, the 4-CP could be efficiently degraded in the system mediated by multiple free radicals, and the reaction rate remained nearly constant across three cycle tests. This was due to the fact that both the original 4-CP and generated intermediates could be rapidly converted and effectively decomposed into $H_2O$ and $CO_2$ etc. Thus there was no electrode fouling in the system mediated by multiple free radicals, and the electrode surface was kept consistently fresh. However, in the absence of one or two types of free radicals, the 4-CP conversion rate gradually decreased over the next three degradation cycles. This decrease was caused by incremental electrode fouling due to the accumulation of 4-CP and intermediates. Excitingly, upon reintroducing the missing free radical into the system, the electrode fouling was significantly alleviated and the catalytic activity gradually recovered. This occurred because the carbon deposits formed on the electrode surface were disrupted, thereby refreshing the electrode surface, which was referred to electrode self-cleaning or electrode anti-fouling. These results again highlight the requirement for the synergy of multiple free radicals for rapid HOPs conversion and complete mineralization.

To accurately reveal the degradation mechanism of HOPs in the system mediated by multiple free radicals, keeping using 4-CP as a prototype, we systematacially investigated its removal path in such a platform. As shown in Fig. S17, the characteristic peak of 4-CP in the UV—Vis absorption spectrum quickly disappeared in the system mediated by multiple free radicals, with hardly any new peaks appearing during the process. In contrast, in system mediated solely by •OH, it took significantly more time for complete obiteration of the 4-CP peak, and numerous new peaks representing various intermediates emerged consecutively as degradation time was extended. These results suggested that 4-CP could be rapidly converted and decomposed into $CO_2$ and $H_2O$, etc., without any accumulation of intermediates in the system mediated by multiple free radicals. The liquid chromatography mass spectrometer (LC-MS) was subsequently employed to precisely identify the steady and unsteady intermediates formed during 4-CP degradation in different systems. The obtained LC-MS results were summarized, and diagrams of 4-CP degradation paths and critical intermediates content variation in different systems were plotted. As seen in Fig. 4A, within the system mediated by multiple free radicals (gray marked area), the Cl— group in 4-CP molecule was first attacked by H* through nucleophilic addition, resulting in a transient intermediate of $C_6H_6OCl$ (marked as S1). The formed S1 would further convert into $C_6H_5O$ (marked as S2)

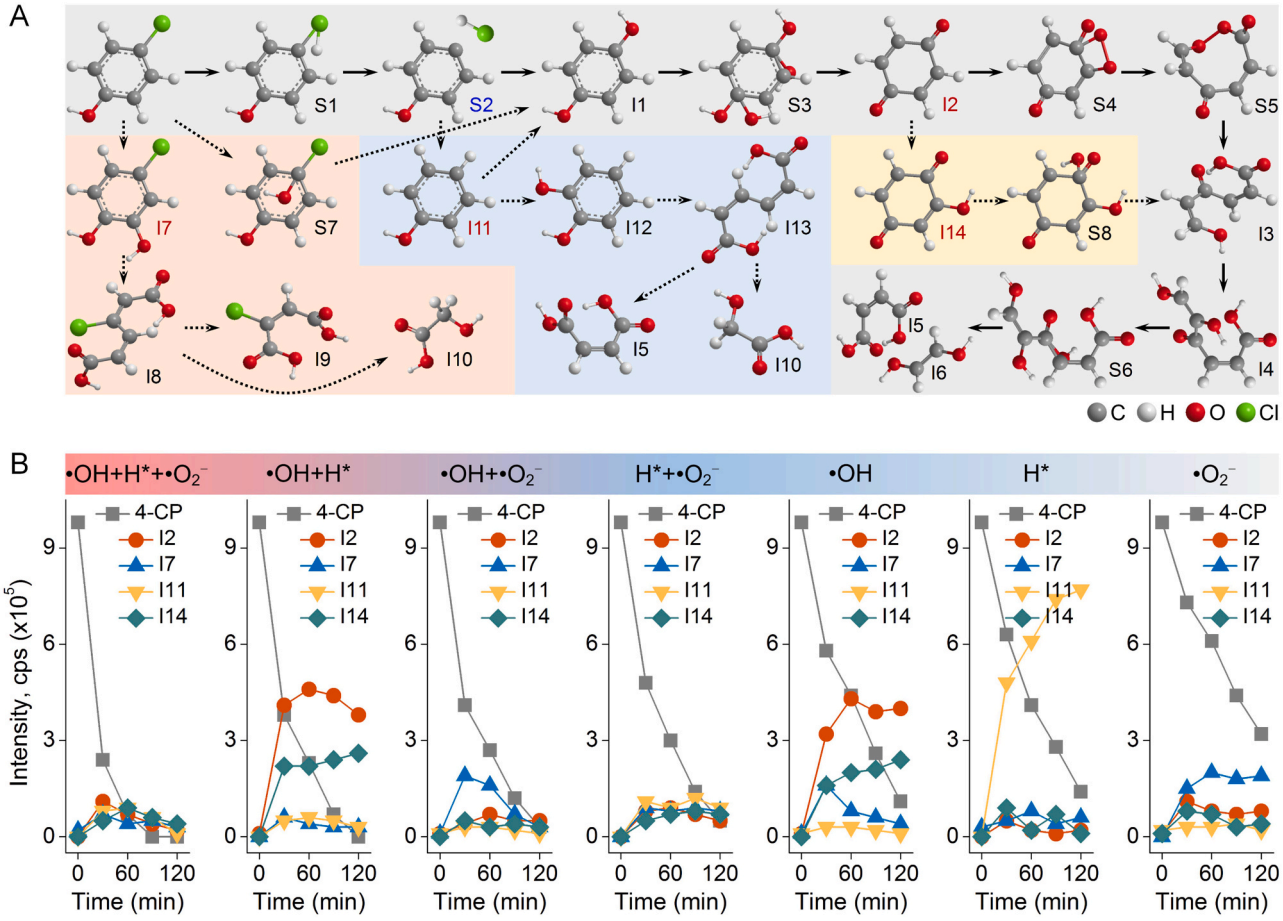


**Fig. 4.** 4-CP removal pathway in $TiO_2$||$Cu_xO$@C/Pd PEC system. (A) 4-CP removal pathway in systems mediated by different combinations of free radicals; (B) Detection of critical intermediates in 4-CP removal processes mediated by different combinations of free radicals. All results were taken from the average of triplicate experiments. Experimental conditions: applied voltage (1.2 V), electrolyte (0.1 M $Na_2SO_4$), 4-$CP_0$ (10 mg $L^{-1}$), air condition, temperature (25 °C), light irradiation.

and HCl by breaking the C—Cl bond. Newly exposed carbon atoms in unsteady S2 were highly prone to attracting a •OH due to its strong electron donating capability, thus forming a steady intermediate of HQ (marked as I1). The conversion from HQ to BQ (marked as I2) went through only one unsteady intermediate of $C_6H_8O_4$ (marked as S3). The ring-opening of BQ required the power of $•O_2^-$, which acted as both an electron donor and acceptor simultaneously, and add to the carbon atoms in and adjacent to the C═O bond through synchronous electrophilic and nucleophilic addition. The generated unsteady intermediate of $C_6H_4O_4$ (marked as S4) quickly converted into another unsteady allotrope of $C_6H_4O_4$ (marked as S5) via the cleavage of the C—C bond that bound $•O_2^-$. After the conversion of S5 to the steady intermediate of $C_6H_6O_4$ (marked as I3) by O—O bond rupture, the subsequent conversion and mineralization of these straight chain aliphatic hydrocarbon intermediates was mainly due to •OH mediated electrophilic oxidation processes. Specifically, I3 trapped a •OH to converte into $C_6H_6O_5$ (marked as I4), and the formed I4 further split into two parts, including $C_4H_4O_4$ (marked as I5) and $C_2H_4O_2$ (marked as I6), which passed through one unsteady intermediate of $C_6H_7O_6$ (marked as S6). Finally, I5 and I6 could be easily mineralized into $CO_2$ and $H_2O$ etc. In general, the degradation path of 4-CP, as mediated by multiple free radicals, was thermodynamically gentle, resulting in these above-mentioned intermediates being detectable, but not accumulating in the system (Fig. 4B). In contrast, the removal of 4-CP as mediated by one/two-component free radicals faced high reaction energy barrier challenges, This resulted in the generation of a variety of intermediates, the majority of which stubbornly persisted in the system for extended periods of time. Specifically, the lack of H* in systems mediated solely or jointly by •OH and $•O_2^-$ seriously lowered the initial 4-CP conversion rate, leading to the accumulation of 4-CP and intermediates such as $C_6H_5O_2Cl$ (marked as I7). In systems mediated by •OH and H* alone or together (without $•O_2^-$), there was no significant impact on the initial 4-CP conversion rate, but there was a notable accumulation of I2 and $C_6H_4O_3$ (marked as I14) among other intermediates, leading to unsatisfactory mineralization efficiency. Indeed, •OH was most critical and permeated the entire HOPs degradation process, including the initial 4-CP conversion and mineralization of intermediates such as I2, I5, I6, I7, $C_6H_6O$ (marked as I11), and I14 etc. This component proved indispensable.

### 3.4. *Effluent quality, durability, and nonspecific substrate feasibility of system mediated by multiple free radicals*

To verify the safety of the final effluent water quality, we assessed changes in the biotoxicity of the 4-CP solution during treatment. First, evaluation results obtained from quantitative structure-activity relationship (QSAR) analyses using the Toxicity Estimation Software Tool (T.E.S.T.) consensus method showed that the most frequently produced intermediates during 4-CP degradation possessed significantly more potential acute toxicity and mutagenicity than the original 4-CP (Fig. 5A) [24,36]. Therefore, complete removal of these intermediates was crucial to ensuring the water quality safety of the final effluent. Further, we conducted growth inhibition assays using luminescent bacteria as a model (Fig. 5B), in-vitro antibacterial assays using Escherichia coli (*E. coli*, gram-negative) and Staphylococcus aureus (*S. aureus*, gram-positive) as models (Fig. 5C), and teratogenicity analyses using zebrafish embryo as a model (Fig. S18) [37–39]. These tests corroborated that 4-CP first decomposed into obviously biotoxic intermediates and then further mineralized into bio-safe $CO_2$ and $H_2O$.

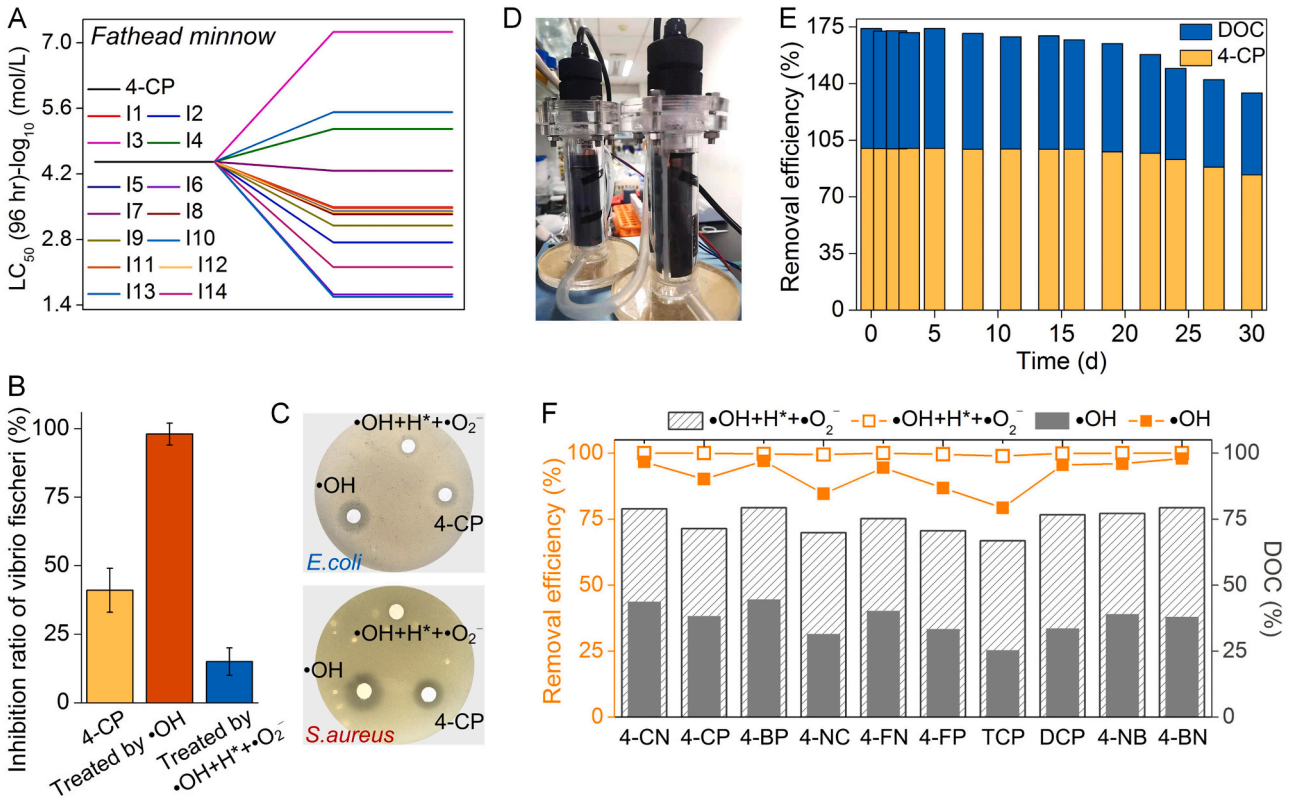


**Fig. 5.** Effluent quality, durability, and nonspecific substrate feasibility of $TiO_2$||$Cu_xO$@C/Pd PEC platform. Toxicity assessments of 4-CP and its degradation products; (A) The QSAR analyses obtained by T.E.S.T. with consensus method; The growth inhibition assays using (B) luminescent bacteria as model and (C) in-vitro antibacterial assays using *E. coli* and *S. aureus* as models; (D) Image of a proof-of-concept $TiO_2$||$Cu_xO$@C/Pd PEC continuous-flow reactor; (E) Stability evaluation via continuously operating for one month; (F) The conversion and mineralization during the degradation of selected several typical HOPs mediated by different free radicals. All results were taken from the average of triplicate experiments. Experimental conditions: applied voltage (1.2 V), electrolyte (0.1 M $Na_2SO_4$), 4-$CP_0$ (10 mg $L^{-1}$), air condition, temperature (25 °C), light irradiation.

These results are consistent with the earlier described 4-CP degradation pathway analyses. In addition, we conducted a long-time flow-running 4-CP degradation to highlight the exceptional durability of the system mediated by multiple free radicals (Fig. 5D). It was apparent that the 4-CP removal efficiency remained nearly constant over a long period (~15 days) (Fig. 5E). Moreover, the contents of leached Ti, Cu, and Pd ions in the treated effluent (<0.05 mg $L^{-1}$) was far below the drinking water permissible limit set by the US Environmental Protection Agency [20,21]. Beyond 4-CP, several other typical HOPs were selected as target emerging pollutants and investigated their removing effectiveness to demonstrate the nonspecific substrate feasibility of the system (Fig. S19). Whether the substituent was fluorine, chlorine or bromine, these varied toxic and harmful substance could be degraded highly efficiently (~100%) within such a platform (Fig. 5F). Furthermore, the HOPs in river water or lake water were almost entirely removed (>90%) after treatment in the system mediated by multiple free radicals, concretely verifying the feasibility of this platform in practical applications (Fig. S20). In addition to HOPs, we have further investigated the removal efficiencies of some other environmental pollutants using current PEC platform (Fig. S21). It was clear that these pollutants were effectively degraded and the rates of conversion and mineralization were as high as ~100% and ~70%, respectively, further confirming the its feasibility for practical application.

### 3.5. Environmental implications

Rapid urbanization and industrialization inevitably produce large amounts of wastewater [40,41]. The current mainstream wastewater treatment technology, the activated sludge process, struggles to remove most refractory organic contaminants in wastewater, including HOPs, which originated from the widespread use of arene, acting as bulk commodity chemicals, in industry, agriculture, and daily life [42,43]. Most HOPs are typically persistent and bioaccumulative in organisms. Once discharged into the environment, these contaminants can cause serious water pollution as well as potentially threaten both ecology and human health. In response to current demands for a more sustainable society, it is imperative to develop efficient emerging technologies to handle sewage containing HOPs. Our experiment and calculation results indicate that the system mediated by multiple free radicals reported in this work is highly suitable for treating wastewater containing HOPs due to the fast conversion and complete mineralization of HOPs. Fig. 6**A** illustrates the complete processing routes from industrial wastewater containing HOPs to clean water, where the one-component •OH mediated and multiple free radicals mediated approaches are adopted respectively. We know that •OH is weak for the preliminary conversion of HOPs due to a high reaction energy barrier, and the produced BQ intermediates are also hard to be further decomposed by •OH, resulting in a low removal rate and mineralization efficiency. Consequently, the effluent from one-component •OH mediated system is substandard for water reuse or discharge into rivers, lakes, and other natural water bodies. In contrast, in the system mediated by multiple free radicals, HOPs can be converted rapidly and leave minimal residual pollutants, including BQ, in the effluent. This ensures the safety of water quality for reuse or discharge.

Ensuring sustainable future energy demand and environmental health has globally attracted increasing attention [44–46]. This goal requires that the energy consumption and environmental impact be considered when developing emerging wastewater treatment technologies, thereby coordinating the energy-environment nexus. Accordingly, we analyzed the pathway and sustainability of the multiple free radicals mediated wastewater treatment process reported in this work, as shown in Fig. S22. It is clear that the electric energy consumption is the only key factor influencing the overall economic and sustainable performances of this process. We then conducted a full life cycle assessment (LCA) with power consumption as the boundary to highlight the economic viability and sustainability of the process mediated by multiple free radicals [47–49]. It is evident that the primary energy demand (PED) in terms of the multiple free radicals mediated 4-CP removal process (complete mineralization) is only about a third as much as one-component •OH mediated approach (Fig. 6B). Further, we calculated and compared the economic costs (Fig. 6C), greenhouse gas ($CO_2$) emissions, eutrophication (EP), ecotoxicity (ET), and acidification (AP) etc. (Fig. 6D) associated with the consumed electric energy in two different approaches. The trend is consistent with the electric energy consumption. Specifically, the multiple free radicals mediated system also demonstrated smaller expenditure and environmental footprints than the one-component •OH

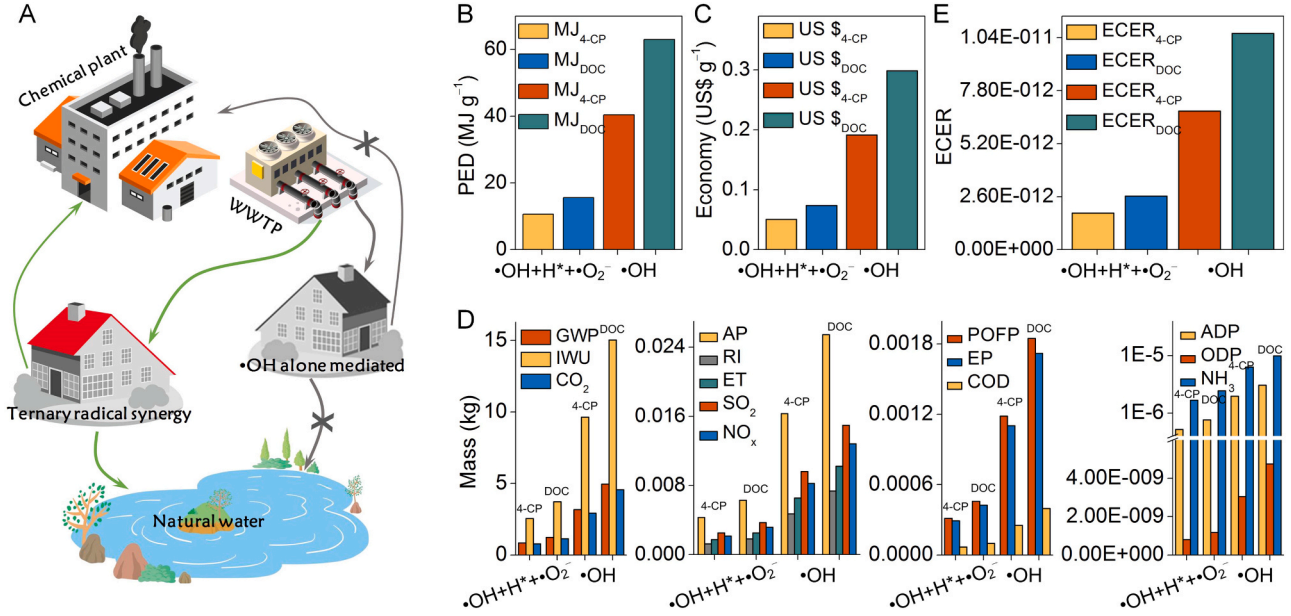


**Fig. 6.** Environmental implications. (A) Schematic drawing of the treatment process flow of wastewater containing HOPs contaminants, in which the one-component •OH mediated PEC process and multiple free radicals mediated PEC process served as core treatment unit, respectively; Comparative LCA associated with the electric energy consumption in different types of free radicals mediated PEC process, including (B) energy consumption, (C) economic costs, (D) greenhouse gas emissions, resource, ecosystem, and human health, and (E) comprehensive influence.

mediated system. Additionally, the multiple free radicals mediated system exhibited overwhelming superiority in other midpoint categories, including scarcity of mineral resource, terrestrial ecotoxicity and human carcinogenic toxicity (Fig. 6E). The overall life-cycle impacts of the multiple free radicals mediated system on human health, ecosystems and resources were less than those of the one-component •OH mediated system. In short, the multiple free radicals mediated system potentiates effective mineralization of HOPs, ensures the safety of effluent water quality, lowers electric energy consumption, saves economic costs, and reduces greenhouse gas equivalents. As such, it demonstrates economic viability and sustainability for wastewater treatment.

## 4. Conclusions

In summary, we have initially carried out the theoretical calculation to prove that the one-component •OH struggles to degrade 4-CP, a typical HOPs, but applying an innovative multiple free radical (H*, $\bullet O_2^-$, and •OH) mediated platform can achieve efficient conversion and mineralization of 4-CP. The reason was that the carbon atoms in the 4-CP molecule exhibit weak electron donating ability due to the strong electronegativity of chloro-substituted groups. This results in a high conversion barrier of up to ~2.51 eV for the electrophilic addition of 4-CP by •OH. Moreover, 4-CP is readily converted to a BQ intermediate, which is difficult to decompose by •OH ($\Delta G$ as high as ~2.12 eV). The strong polarity of carbonyl groups (C═O) in the BQ molecule induces an uneven electron distribution, resulting in opposite redox characteristics for the adjacent carbon atoms. In contrast, the conversion barrier of 4-CP is significantly reduced to ~0.91 eV through a redox synergistic process of H* -initiating nucleophilic hydrodechlorination followed by •OH electrophilic oxidization of critical intermediate. Meanwhile, the introduced $\bullet O_2^-$ acts simultaneously as an electron donor and acceptor simultaneously, and it both electrophilically and nucleophilically adds to BQ synchronously ($\Delta G$ = ~1.42 eV). This effectively inhibits BQ accumulation. Subsequently, we architected a $TiO_2$‖$Cu_xO$@C/Pd PEC platform that achieves synchronous generation and efficient coexistence of H* , $\bullet O_2^-$, and •OH. The •OH generated on the $TiO_2$ surface by one-electron WOR, while $Cu_xO$@C/Pd simultaneously produced H* and $\bullet O_2^-$ via the hydrogen fixation (Volmer) and MOA processes, respectively. In this platform, we further confirmed that the synergy of multiple free radical effectively degrades 4-CP and other HOPs. The conversion and mineralization rates in the multiple free radical mediated system were more than four times higher than in the one-component •OH mediated system. More importantly, the synergy of multiple free radicals also effectively improved electrode stability, reduced effluent toxicity, saved energy and costs, and decreased environmental footprint, as evidenced by the LCA.

## Author contribution statement

Jun Zhang and Songying Qu conceived the idea and led the project; Jun Zhang and Songying Qu designed and performed experiments; Jun Zhang and Songying Qu analyzed characterization data; Jun Zhang and Songying Qu analyzed experimental results; Jun Zhang developed analysis tools; Jun Zhang and Songying Qu wrote the manuscript.

## CRediT authorship contribution statement

**Qu Songying:** Conceptualization, Methodology, Supervision, Writing – review & editing. **Zhang Jun:** Conceptualization, Investigation, Methodology, Resources, Writing – original draft.

## Declaration of Competing Interest

The authors declare that they have no known competing financial interests or personal relationships that could have appeared to influence the work reported in this paper.

## Data Availability

No data was used for the research described in the article.

## Acknowledgments

This work was financially supported by National Natural Science Foundation of China (No. 52300096), the China Postdoctoral Science Foundation (2023M731933), China State-sponsored Postdoctoral Researcher Program Grade B, and “Shuimu Tsinghua Scholar” Support Plan.

## Appendix A. Supporting information

Supplementary data associated with this article can be found in the online version at doi:10.1016/j.apcatb.2023.123554.

## References

[1] B.C. Hodges, E.L. Cates, J.H. Kim, Challenges and prospects of advanced oxidation water treatment processes using catalytic nanomaterials, Nat. Nanotechnol. 13 (2018) 642–650.
[2] J.W. Xu, X.L. Zheng, Z.P. Feng, Z.Y. Lu, Z.W. Zhang, W. Huang, Y.B. Li, D. Vuckovic, Y.Q. Li, S. Dai, G.X. Chen, K.C. Wang, H.S. Wang, J.K. Chen, W. Mitch, Y. Cui, Organic wastewater treatment by a single-atom catalyst and electrolytically produced $H_2O_2$, Nat. Sustain. 4 (2021) 233–241.
[3] D.B. Miklos, C. Remy, M. Jekel, K.G. Linden, J.E. Drewes, U. Hubner, Evaluation of advanced oxidation processes for water and wastewater treatment-A critical review, Water Res 139 (2018) 118–131.
[4] J.D. Xiao, Y.B. Xie, J. Rabeah, A. Bruckner, H.B. Cao, Visible-light photocatalytic ozonation using graphitic $C_3N_4$ catalysts: a hydroxyl radical manufacturer for wastewater treatment, Acc. Chem. Res. 53 (2020) 1024–1033.
[5] R. Song, H.B. Chi, Q.L. Ma, D.F. Li, X.M. Wang, W.S. Gao, H. Wang, X.L. Wang, Z. L. Li, C. Li, Highly efficient degradation of persistent pollutants with 3D nanocone TiO2-based photoelectrocatalysis, J. Am. Chem. Soc. 143 (2021) 13664–13674.
[6] F. Xiao, Z.N. Wang, J.Q. Fan, T. Majima, H.Y. Zhao, G.H. Zhao, Selective electrocatalytic reduction of oxygen to hydroxyl radicals via 3-electron pathway with FeCo alloy encapsulated carbon aerogel for fast and complete removing pollutants, Angew. Chem. Int. Ed. 60 (2021) 10375–10383.
[7] Z. Guo, Y.B. Xie, J.D. Xiao, Z.J. Zhao, Y.X. Wang, Z.M. Xu, Y. Zhang, L.C. Yin, H. B. Cao, J.L. Gong, Single-atom Mn-$N_4$ site-catalyzed peroxone reaction for the efficient production of hydroxyl radicals in an acidic solution, J. Am. Chem. Soc. 141 (2019) 12005–12010.
[8] X. Qin, P.K. Cao, X. Quan, K. Zhao, S. Chen, H.T. Yu, Y. Su, Highly efficient hydroxyl radicals production boosted by the atomically dispersed Fe and Co sites for heterogeneous electro-Fenton oxidation, Environ. Sci. Technol. 57 (2023) 2907–2917.
[9] H.B. Zeng, G. Zhang, Q.H. Ji, H.J. Liu, X. Hua, H.L. Xia, M. Sillanpaa, J.H. Qu, pH-independent production of hydroxyl radical from atomic H*-mediated electrocatalytic $H_2O_2$ reduction: A green Fenton process without byproducts, Environ. Sci. Technol. 54 (2020) 14725–14731.
[10] D.N. Pei, C. Liu, A.Y. Zhang, X.Q. Pan, H.Q. Yu, In situ organic Fenton-like catalysis triggered by anodic polymeric intermediates for electrochemical water purification, Proc. Natl. Acad. Sci. U. S. A. 117 (2020) 30966–30972.
[11] J.J. Zhang, X. Zhao, Y. Wang, R. Djellabi, Recovery of phosphorus from hypophosphite-laden wastewater: a single-compartment photoelectrocatalytic cell system integrating oxidation and precipitation, Environ. Sci. Technol. 54 (2020) 1204–1213.
[12] Y. Chen, G. Zhang, H.J. Liu, J.H. Qu, Confining free radicals in close vicinity to contaminants enables ultrafast Fenton-like processes in the interspacing of $MoS_2$ membranes, Angew. Chem. Int. Ed. 58 (2019) 8134–8138.
[13] C.C. Meng, B.F. Ding, S.Z. Zhang, L.L. Cui, K.K. Ostrikov, Z.Y. Huang, B. Yang, J. H. Kim, Z.H. Zhang, Angstrom-confined catalytic water purification within Co-$TiO_x$ laminar membrane nanochannels, Nat. Commun. 13 (2022) 4010.
[14] M.J. Xu, Y. Chen, J.T. Qin, Y.W. Feng, W. Li, W. Chen, J. Zhu, H.X. Li, Z.F. Bian, Unveiling the role of defects on oxygen activation and photodegradation of organic pollutants, Environ. Sci. Technol. 52 (2018) 13879–13886.
[15] D.D. Zhou, S.S. Dong, J.L. Shi, X.C. Cui, D.W. Ki, C.I. Torres, B.E. Rittmann, Intimate coupling of an N-doped $TiO_2$ photocatalyst and anode respiring bacteria for enhancing 4-chlorophenol degradation and current generation, Chem. Eng. J. 317 (2017) 882–889.
[16] N.B. Zhong, M. Chen, Y.H. Luo, Z.K. Wang, X. Xin, B.E. Rittmann, A novel photocatalytic optical hollow-fiber with high photocatalytic activity for enhancement of 4-chlorophenol degradation, Chem. Eng. J. 355 (2019) 731–739.
[17] Y.Y. Chu, X.L. Zheng, J.R. Fan, Preparation of sodium and boron co-doped graphitic carbon nitride for the enhanced production of $H_2O_2$ via two-electron oxygen reduction and the degradation of 2,4-DCP via photocatalytic oxidation coupled with Fenton oxidation, Chem. Eng. J. 431 (2022), 134020.
[18] Z.S. Chen, W.R. Chen, G.Z. Liao, X.K. Li, J. Wang, Y.M. Tang, L.S. Li, Flexible construct of N vacancies and hydrophobic sites on g-$C_3N_4$ by F doping and their

contribution to PFOA degradation in photocatalytic ozonation, J. Hazard. Mater. 428 (2022), 128222.
[19] M.V. Carevic, N.D. Abazovic, T.B. Novakovic, V.B. Pavlovic, M.I. Comor, Zirconium dioxide nanopowders with incorporated $Si^{4+}$ ions as efficient photocatalyst for degradation of trichlorophenol using simulated solar light, Appl. Catal. B Environ. 195 (2016) 112–120.
[20] J. Zhang, Q.H. Ji, H.C. Lan, G. Zhang, H.J. Liu, J.H. Qu, Synchronous reduction-oxidation process for efficient removal of trichloroacetic acid: H* initiates dechlorination and •OH is responsible for removal efficiency, Environ. Sci. Technol. 53 (2019) 14586–14594.
[21] P. Liu, B. Chen, C.W. Liang, W.T. Yao, Y.Z. Cui, S.Y. Hu, P.C. Zou, H. Zhang, H. J. Fan, C. Yang, Tip-enhanced electric field: a new mechanism promoting mass transfer in oxygen evolution reactions, Adv. Mater. 33 (2021) 2007377.
[22] C.Y. Guo, P. He, R.R. Cui, Q. Shen, N.J. Yang, G.H. Zhao, Electrochemical $CO_2$ reduction using electrons generated from photoelectrocatalytic phenol oxidation, Adv. Energy Mater. 9 (2019) 1900364.
[23] C.L. Liu, W. Zhou, J.K. Song, H.J. Liu, J.H. Qu, L. Guo, G.F. Song, C.P. Huang, Nanostructure-induced colored $TiO_2$ array photoelectrodes with full solar spectrum harvesting, J. Mater. Chem. A 5 (2017) 3145–3151.
[24] J. Zhang, G. Zhang, H.C. Lan, H.J. Liu, J.H. Qu, Selective oxygen activation to reactive oxygen species on a carbon layer-encapsulated $Cu_xO$ electrocatalyst for water purification, Environ. Sci. Technol. 57 (2023) 1134–1143.
[25] R. Liu, H.C. Zhao, X.Y. Zhao, Z.L. He, Y.J. Lai, W.Y. Shan, D. Bekana, G. Li, J.F. Liu, Defect sites in ultrathin Pd nanowires facilitate the highly efficient electrochemical hydrodechlorination of pollutants by H*(ads), Environ. Sci. Technol. 52 (2018) 9992–10002.
[26] K. Zhao, L.Z. Zhang, J.J. Wang, Q.X. Li, W.W. He, J.J. Yin, Surface structure-dependent molecular oxygen activation of BiOCl single-crystalline nanosheets, J. Am. Chem. Soc. 135 (2013) 15750–15753.
[27] J. Zhang, G. Zhang, H.C. Lan, H.J. Liu, J.H. Qu, Sustainable nitrogen fixation over Ru single atoms decorated $Cu_2O$ using electrons produced from photoelectrocatalytic organics degradation, Chem. Eng. J. 428 (2022), 130373.
[28] C.R. Dong, Y.L. Yang, X.M. Hu, Y. Cho, Y.Y. Jang, Y.H. Ao, L.Y. Wang, J.Y. Shen, J. H. Park, K. Zhang, Self-cycled photo-Fenton-like system based on an artificial leaf with a solar-to-$H_2O_2$ conversion efficiency of 1.46%, Nat. Commun. 13 (2022) 4982.
[29] X.J. Shi, Y.R. Zhang, S. Siahrostami, X.L. Zheng, Light-driven $BiVO_4$-C fuel cell with simultaneous production of $H_2O_2$, Adv. Energy Mater. 8 (2018) 1801158.
[30] Y. He, K.D. Chen, M.K.H. Leung, Y.Z. Zhang, L. Li, G.S. Li, J. Xuan, J.F. Li, Photocatalytic fuel cell-A review, Chem. Eng. J. 428 (2022), 131074.
[31] J. Zhou, M. Wen, R. Huang, Q.S. Wu, Y.X. Luo, Y.K. Tian, G.F. Wei, Y.Q. Fu, Regulating active hydrogen adsorbed on grain boundary defects of nano-nickel for boosting ammonia electrosynthesis from nitrate, Energy Environ. Sci. 16 (2023) 2611–2620.
[32] X.M. Xu, Y.M. Zhang, Y. Chen, C.H. Liu, W.J. Wang, J.J. Wang, H.T. Huang, J. Y. Feng, Z.S. Li, Z.G. Zou, Revealing *OOH key intermediates and regulating $H_2O_2$ photoactivation by surface relaxation of Fenton-like catalysts, Proc. Natl. Acad. Sci. U. S. A. 119 (2022) 2205562119.
[33] W. Zhang, Y. Chen, G. Zhang, X. Tan, Q.H. Ji, Z.W. Wang, H.J. Liu, J.H. Qu, Hot-electron-induced photothermal catalysis for energy-dependent molecular oxygen activation, Angew. Chem. Int. Ed. 60 (2021) 4872–4878.
[34] J. Li, G.M. Zhan, J.H. Yang, F.J. Quan, C.L. Mao, Y. Liu, B. Wang, F.C. Lei, L.J. Li, A. W.M. Chan, L.P. Xu, Y.B. Shi, Y. Du, W.C. Hao, P.K. Wong, J.F. Wang, S.X. Dou, L. Z. Zhang, J.C. Yu, Efficient ammonia electrosynthesis from nitrate on strained ruthenium nanoclusters, J. Am. Chem. Soc. 142 (2020) 7036–7046.
[35] H.H. Qin, X.J. Wei, Z.W. Ye, X.Y. Liu, S. Mao, Promotion of phenol electro-oxidation by oxygen evolution reaction on an active electrode for efficient pollution control and hydrogen evolution, Environ. Sci. Technol. 56 (2022) 5753–5762.
[36] J.J. Jiang, Z.Q. Zhao, J.Y. Gao, T.R. Li, M.Y. Li, D.D. Zhou, S.S. Dong, Nitrogen vacancy-modulated peroxymonosulfate nonradical activation for organic contaminant removal via high-valent cobalt-oxo species, Environ. Sci. Technol. 56 (2022) 5611–5619.
[37] J. Zhang, Y. Guo, Y.H. Xiong, D.D. Zhou, S.S. Dong, An environmentally friendly Z-scheme $WO_3$/CDots/CdS heterostructure with remarkable photocatalytic activity and anti-photocorrosion performance, J. Catal. 356 (2017) 1–13.
[38] X.P. Wu, J. Zhang, S.C. Hu, G. Zhang, H.C. Lan, J.F. Peng, H.J. Liu, Evaluation of degradation performance toward antiviral drug ribavirin using advanced oxidation process and its relations to ecotoxicity evolution, Sci. Total Environ. 850 (2022), 157851.
[39] P.S. Priya, A. Guru, R. Meenatchi, B. Haridevamuthu, M. Velayutham, B. Seenivasan, R. Pachaiappan, R. Rajagopal, P. Kuppusamy, A. Juliet, J. Arockiaraj, Syringol, a wildfire residual methoxyphenol causes cytotoxicity and teratogenicity in zebrafish model, Sci. Total Environ. 864 (2023), 160968.
[40] J.H. Qu, H.J. Liu, G. Liu, Science and technology for combating global water challenges, Engineering 9 (2022) 1–2.
[41] K. Kummerer, D.D. Dionysiou, O. Olsson, D. Fatta-Kassinos, A path to clean water, Science 361 (2018) 222–224.
[42] R. Jin, M.H. Zheng, G. Lammel, B.A.M. Bandowe, G.R. Liu, Chlorinated and brominated polycyclic aromatic hydrocarbons: sources, formation mechanisms, and occurrence in the environment, Prog. Energy Combust. Sci. 76 (2020), 100803.
[43] Y. Guo, Y. Li, Z.W. Wang, Electrocatalytic hydro-dehalogenation of halogenated organic pollutants from wastewater: a critical review, Water Res 234 (2023), 119810.
[44] S. Chu, A. Majumdar, Opportunities and challenges for a sustainable energy future, Nature 488 (2012) 294–303.
[45] J. Baleta, H. Mikulcic, J.J. Klemes, K. Urbaniec, N. Duic, Integration of energy, water and environmental systems for a sustainable development, J. Clean. Prod. 215 (2019) 1424–1436.
[46] J.J. Urban, Emerging scientific and engineering opportunities within the water-energy nexus, Joule 1 (2017) 665–688.
[47] S. Hellweg, L.M.I. Canals, Emerging approaches, challenges and opportunities in life cycle assessment, Science 344 (2014) 1109–1113.
[48] S. Zhang, S.F. Jiang, B.C. Huang, X.C. Shen, W.J. Chen, T.P. Zhou, H.Y. Cheng, B. H. Cheng, C.Z. Wu, W.W. Li, H. Jiang, H.Q. Yu, Sustainable production of value-added carbon nanomaterials from biomass pyrolysis, Nat. Sustain. 3 (2020) 753–760.
[49] Y. Sun, S.W. Bai, X.H. Wang, N.Q. Ren, S.J. You, Prospective life cycle assessment for the electrochemical oxidation wastewater treatment process: from laboratory to industrial scale, Environ. Sci. Technol. (2023) 1456–1466.